Analysis of Nonlinear Left-Handed Transmission Lines Using State Space Modelling

Sameh Y. Elnaggar
School of Engineering and Information Technology
University of New South Wales
Canberra
Email: s.elnaggar@unsw.edu.au

G. N. Milford
School of Engineering and Information Technology
University of New South Wales
Canberra
Email: g.milford@adfa.edu.au

Abstract—**In this paper we demonstrate the use of state space modelling for analysing parametric generation in nonlinear composite right left handed transmission lines. The system natural frequencies are identified and found to be comparable to the dominant poles of the linearized system. With an input pump excitation, the structure generates parametric frequency components, and the state space analysis suggests that the values of the parametric frequencies are determined by the dominant poles of the linearized system. The growth of the parametric components depends on the net effect of the energy transfer from the pump and the dissipative nature of the structure. It is found that below a threshold value of the pump amplitude, the parametric components are inhibited. This threshold value is a function of the pump frequency and the structure losses. The numerical calculations are in good agreement with measurements. State space formulations allow the application of the mature and robust techniques of systems and control methodologies to analyse the behaviour of nonlinear right left handed transmission line systems.**

I. Introduction

Left-handed or Composite Right-Left handed transmission lines (CRLH TL) have been extensively studied in the literature [1], [2]. Such structures were shown to have lower losses and wider bandwidth than resonance based systems [1]. The combination of left and right-handed propagation behaviour introduces a paradigm that is useful for the design of microwave devices, such as broadband directional couplers [3], leaky-wave antenna with tunable radiation angle and beamwidth [4] and super-resolution lenses that overcome the diffraction limit [5]. The introduction of nonlinear reactive components to a CRLH TL produces nonlinear amplitude behaviour. It has been demonstrated that nonlinear (NL) CRLH TL based structures display interesting phenomena such as harmonic, subharmonic and parametric generation [8], envelope solitons [9] and multistabilty [10]. In particular, the parametric interactions in NL CRLH TL structures between a strong (pump) and a weak (signal) inputs [6] offer the potential for very low noise distributed amplifiers and oscillators at mm-wave and terahertz frequencies. However, improvements in the understanding of the parametric generation process are needed to enable design of efficient parametric signal processing components.
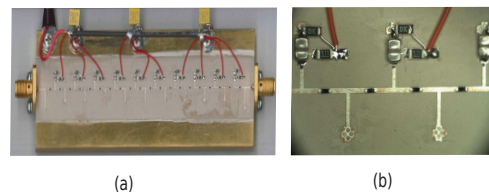

Fig. 1. (a) The 20 stages NL CRLH TL. (b) Zoomed view showing the varactor connection and biasing circuitry.

State space models (SSMs) were developed to study CRLH TLs [11]. In this approach, the distributed line was modelled by series and shunt lumped circuit elements. In general, SSMs cast the problem in an $\dot{x} = f(x, t)$ form which permits the mature and robust techniques of control and systems theory to be applied. Moreover, SSMs are time domain models which are necessary for studying nonlinear systems and arbitrary input excitations.

In this paper, we illustrate the use of a nonlinear SSM to describe parametric frequency generation in a NL CRLH TL. The relationship between the parametric frequencies and the linearized system's poles is established. The paper is organized as follows: Section II describes the NL CRLH TL schematics and the SSM. The linearization of the SSM is carried out in Section III where the system poles are calculated. Section IV presents the impulse response and the natural frequencies of the NL CRLH TL. Section V discusses parametric frequency values and the connection with the natural frequencies of the system.

II. State Space Model of Nonlinear TL

The NL CRLH TL, shown in Fig. 1, consists of a cascade of 20 unit cells, where each unit cell has a series varactor C_L, where this capacitance is a function of the terminal voltages. Fig. 2 shows a lumped element equivalent circuit model of the NL CRLH TL. As Fig. 2 shows, V_b is applied to reverse bias the varactors. The right handed circuit parameters L_R and C_R are 2.7 nH and 1.1 pF, respectively. The left-handed inductance $L_L = 1.797$ nH. The varactor capacitance is determined by:
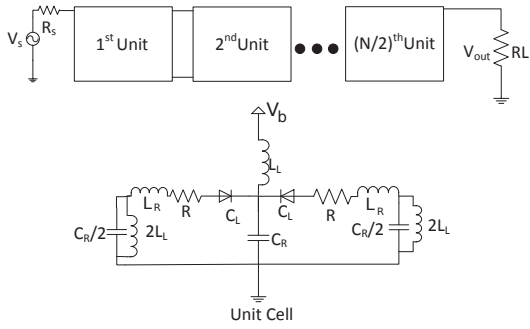
Fig. 2. The lumped circuit model of the NL CRLH TL. For biasing reasons, each unit cell of the nonlinear circuit is comprised of two cascaded sub-units and hence the number of unit cells is N/2.

$$C_L = \frac{C_{j0}}{\left(1 - \frac{v}{\psi_0}\right)^{\gamma}}, \qquad (1)$$

where $C_{j0} = 1.33$ pF, $\psi_0 = 4.07$ V, $\gamma = 2.1$ and v is the reverse voltage across the varactor's terminals. A bias voltage of ≈ 1.4 V reverse biases the varactors and produces a balanced frequency response. The state space equation:

$$\dot{\boldsymbol{x}} = \boldsymbol{f}(\boldsymbol{x}, t) \qquad (2)$$

can be found by applying KVL and KCL. In (2), $\boldsymbol{x}$ is the state variable vector. The SSM of the NL CRLH TL can be written as:

$$\dot{\boldsymbol{x}} = \boldsymbol{A}\boldsymbol{x} + \boldsymbol{B}u + \boldsymbol{F}(\boldsymbol{x})\boldsymbol{x} + \boldsymbol{D}V_b, \qquad (3)$$

where $\boldsymbol{x}$ is a $4N+2$ column vector, $\boldsymbol{A}$ is a $(4N+2) \times (4N+2)$ sparse matrix with elements determined by the circuit topology and $\boldsymbol{B}$ is a $4N+2$ column vector which maps the excitation to the states, having one non-zero element $\boldsymbol{B}(2,1) = 2/C_R R_s$. The nonlinearities are restricted to the sparse $(4N+2) \times (4N+2)$ $\boldsymbol{F}$ matrix, which is a function of the nonlinear capacitance C_L. The non-zero elements of $\boldsymbol{F}$ are given by:

$$\boldsymbol{F}(4m, 4m-1) = \frac{1}{C_L(x(4m,1))}, \qquad (4)$$

for $m = 1, 2, \cdots, N$. It is worth noting that the voltage v in (1) is related to $\boldsymbol{x}(4m, 1)$ by

$$v = (-1)^{m-1}\boldsymbol{x}(4m, 1). \qquad (5)$$

$\boldsymbol{D}$ is a $4N+2$ column vector that explicitly links the DC bias voltage to the states.

III. LINEARIZATION OF THE STATE SPACE MODEL

In this section, the SSM given by (3) is linearized around the equilibrium point, which is defined as $\dot{\boldsymbol{x}} = 0$ or equivalently $\boldsymbol{f}(\boldsymbol{x}, t) = 0$. Through such small signal linearisation we obtain the system eigenvalues, thereby characterising the frequency response, stability and dynamic behaviour of the system at
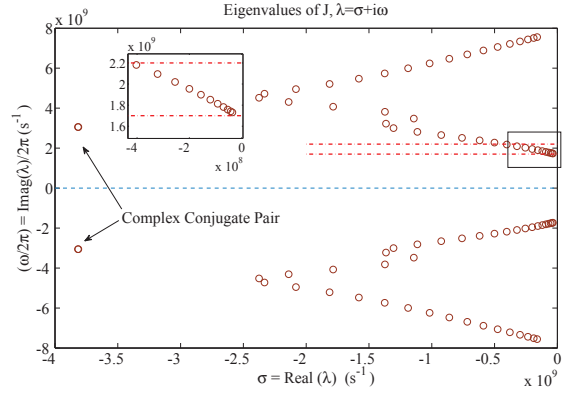

Fig. 3. The eigenvalues $\lambda = \sigma + j\omega$ of the Jacobian matrix $\boldsymbol{J}$ of (7), representing the poles of the NL CRLH TL of (3) linearised about equilibrium point $\dot{\boldsymbol{x}} = 0$.

this equilibrium point in response to disturbances. For the NL CRLH TL shown in Fig. 2, the equilibrium point can be found by applying the bias voltage and waiting until the system reaches steady state. The capacitance C_L of the varactors is determined by setting $v = V_b$ in (1). The linearized system is then determined by finding the Jacobian $\boldsymbol{J}$ of the right hand side of (2), where $\boldsymbol{J}$ is a $(4N + 2) \times (4N + 2)$ matrix with i, j elements given by:

$$\boldsymbol{J}_{ij} = \frac{\partial \boldsymbol{f}_i}{\partial \boldsymbol{x}_j}. \qquad (6)$$

The Jacobian of the NL CRLH TL in (3) is then:

$$\boldsymbol{J}_{ij} = \boldsymbol{A}_{ij} + \boldsymbol{F}'_{ij}, \qquad (7)$$

where $\boldsymbol{F}'_{ij} = 1/C_L(v = V_b)$ when $i = 4m$, $j = i - 1$, $m = 1, 2, \cdots, N$ and is zero elsewhere. The eigenvalues (or poles) of $\boldsymbol{J}$ determine the natural response of the NL CRLH TL structure, and are plotted in Fig. 3.

The time and frequency domain responses of this system are strongly influenced by the lightly damped (dominant) poles around 2 GHz. Indeed as will be seen in Section V, the lowest parametric frequency is located in the area bounded by the two dashed-dotted lines and in the vicinity of the dominant poles. Note that all of the poles appear as complex conjugate pairs.

IV. IMPULSE RESPONSE OF THE LINE

In this section, the SSM given by (3) is solved numerically using Runge-Kutta Method (ODE45, MATLAB®). Fig. 4 shows the time and frequency domain responses of the output voltage. In this configuration the bias voltage was applied at $t = 0$ and a pulse of width 10 ps and height of 10 V was applied to the input at $t = 1.1$ μs. This timing guarantees that the transient response due to the bias is sufficiently small. The
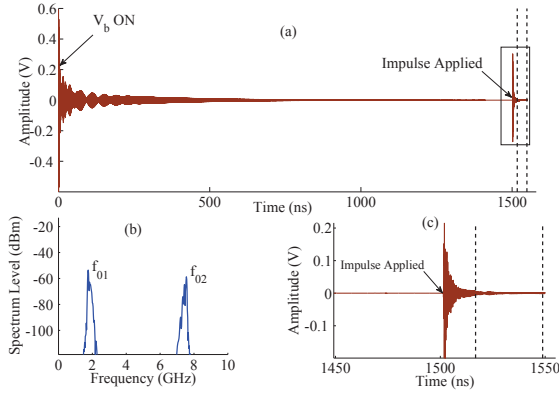
Fig. 4. The impulse response of the NL CRLH TL. The input pulse $V_s = 10$ V applied for 10 ps. The impulse is fired on at $t = 1.5$ μs. (a) The time response. (b) The FFT of the time response over the period [1517-1549] ns. (c) The *zoomed* time response in the box in (a).

Fig. 5. Demonstration of the agreement between (a) the left-hand Bragg frequency f_B of (8), (b) the observed natural frequency f_{01} in Fig. 4 using SSM calculations, and (c) the imaginary component of the smallest eigenvalue (Fig. 3), for a range of C_{jo} values in (1).

spectrum is calculated using a Fourier Transform of the time response over the interval 1517-1549 ns (shown in Fig. 4(c)). The sampling rate is 2 THz.

From the calculated spectrum, it is clear that the main natural frequencies are f_{01} and f_{02}. These frequencies are consistent with the lowest and highest cut off frequencies, respectively, of the bandpass CRLH TL (Fig. 7). To illustrate this correlation, the lower left-handed cut off frequency (Bragg frequency f_B) was calculated for a range of capacitance values (C_{j0} of (1) from 0.33 to 2.00 pF), where from [2]:

$$f_B = f_R \left| 1 - \sqrt{1 + \frac{f_L}{f_R}} \right|, \qquad (8)$$

where $f_R = 1/2\pi\sqrt{L_R C_R}$, $f_L = 1/2\pi\sqrt{L_L C_L}$. Values for the frequency f_{01} are computed from the frequency spectrum after solving the SSM in (3) for each C_L value. These results are shown in Fig. 5 along with the values of the imaginary components of the smallest eigenvalue λ_{min} for each C_L (Fig. 3). There appears to be very good agreement between all three frequencies for each C_L value. Furthermore, the calculated f_{01} frequencies were found to be independent on the pulse height and slightly increase with increasing line resistance R.

The excitation of the frequencies f_{01} and f_{02} can be explained by noting that the input impulse has a broadband frequency response and thus excites the different system poles. However, only the response of lightly damped poles is visible over a relatively long interval. Other responses are quickly damped with a few nano seconds after the application of the impulse.

V. PARAMETRIC GENERATION

To study the parametric behaviour of the NL CRLH TL, a sinewave pump voltage is applied. To avoid transients associated with applicat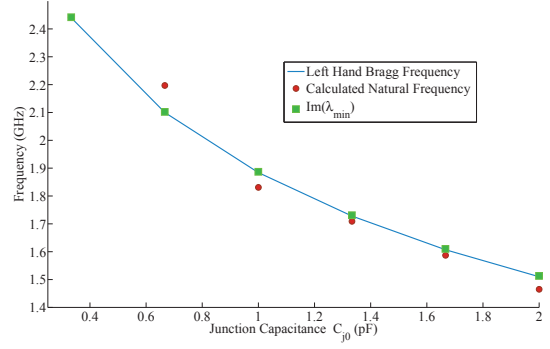ion of the bias voltage, the pump is applied after the line reaches steady state. The spectrum of the output node is calculated for a range of input pump powers. As the pump power is increased above what appears to be a threshold value, there is a rapid growth of spectral components. Two prominent components at frequencies f_1 and f_2 appear in the spectrum where $f_1 + f_2 = f_{pump}$. These components are referred to as the parametric components, and vary with pump frequency as illustrated in the upper plot in Fig. 6.

The lowest parametric frequency f_1 has a value which is very close to f_B, or equivalently f_{01}. Given the comparatively wide range of pump frequencies in Fig. 6, the corresponding range of f_1 values stays within the strip denoted by the two dashed-dotted lines in Fig. 3. Hence, we infer that the lowest parametric frequency is determined by the the frequencies of the dominant poles of the linearized transmission line system. The other parametric frequency f_2 is then uniquely determined by $f_2 = f_{pump} - f_1$. Energy transfer from the pump to the lightly damped poles is facilitated by the nonlinearities in the system. The excitation of dominant poles can be explained by noting that the spectral content of the pump at turn on (just after t = 400 ns) is relatively broadband, thereby exciting the system poles.

The frequencies calculated using SSM and presented in Fig. 6(a) show very good agreement with the experimental values presented in Fig. 6(b) [7]. The SSM predicts that the two parametric frequencies start to diverge when $f_{pump} \approx 4.2$ GHz, whereas the measured frequencies diverge at around $f_{pump} \approx 4.6$ GHz. A number of factors could contribute to this discrepancy. Firstly, the effect of component parasitics, not taken into account in the SSM, alters the system performance, as illustrated by the differences in the steady state frequency responses close to f_B shown in Fig. 7. Secondly, the value of the unit cell resistor R which was taken to be 1 Ω in the SSM, whereas the physical structure would have distributed and not necessarily uniform loss mechanisms. Thirdly, the varactor
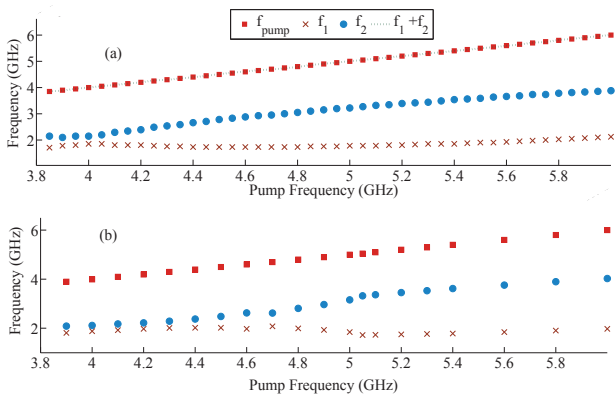
Fig. 6. The two lowest parametric frequencies, f_1 and f_2, for given pump frequencies, f_{pump} using (a) State Space Model, (b) Measurements [7].
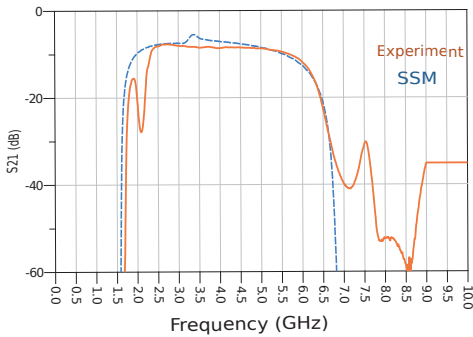

Fig. 7. Small Signal S Parameters for $V_b \approx 1.45$ V (balanced).
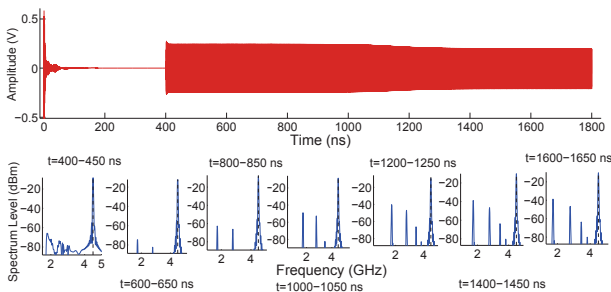

Fig. 8. Parametric frequency generation, $f_{pump} = 4.5$ GHz, $P_{pump} = 5.5$ dBm. Spectra are depicted for the indicated time intervals.

model used here does not include forward bias diffusion capacitance effects.

The parametric generation is the net result of two competing processes. The first is the coupling between the pump and the lightly damped poles. The other suppresses the generation due to the dissipative nature of the structure, reflected in the unit cell resistance R. Fig. 8 shows the time evolution of the output when $f_{pump} = 4.5$ GHz, $P_{pump} = 5.5$ dBm and $R = 1$ Ω. The bias voltage ($V_b = 1.45$V) is turned on at $t = 0$ and the pump at $t = 400$ ns. The 400 ns time lag guarantees that the system reaches steady state before application of the

pump. The time domain waveform shows a slight decrease in envelope amplitude between 1000 ns and 1200 ns, while the gated spectral plots show a gradual evolution of the parametric components, from the initial excitation (400-450 ns window) to steady state around 1500 ns. When R is slightly increased to 1.2 Ω, the parametric frequencies are suppressed. Similarly below $P_{pump} = 5.5$ dBm, the parametric frequencies are not observed.

VI. CONCLUSION

In summary a SSM was developed for time domain analysis of a NL CRLH TL. The SSM approach brings a control theory perspective to the study of the distributed circuit nonlinear left-handed transmission line structure. The SSM was linearized around the equilibrium point, from which the system poles could be identified. It was shown that the lowest parametric frequency is determined by the lightly damped dominant poles of the linearized system. By varying the losses in the SSM the onset of parametric frequency generation with pump power and frequency can be determined. This insight suggests that the dynamic behaviour of parametric frequency generation is a balance between natural response excitation and dissipation by the structure losses. The understanding of the parametric generation process is crucial for the design of efficient parametric amplifiers.

REFERENCES

[1] G. V. Eleftheriades and K. G. Balmain, *Negative-Refraction Metamat erials*. New Jersey: IEEE Press and Wiley-Interscience, 2005.

[2] C. Caloz and T. Itoh, *Electromagnetic Metamaterials*. New Jersey: Wiley-Interscience, 2006.

[3] C. Caloz, A. Sanada, and T. Itoh, *"A novel composite right-/left-handed coupled-line directional coupler with arbitrary coupling level and broad bandwidth,"* Microwave Theory and Techniques, IEEE Transactions on, vol. 52, pp. 980-992, 2004.

[4] S. Lim, C. Caloz, and T. Itoh, *"Metamaterial-based electronically controlled transmission-line structure as a novel leaky-wave antenna with tunable radiation angle and beamwidth,"* Microwave Theory and Techniques, IEEE Transactions on, vol. 53, pp. 161-173, 2005.

[5] A. Grbic and G. V. Eleftheriades, *"Overcoming the Diffraction Limit with a Planar Left-Handed Transmission-Line Lens,"* Physical Review Letters, vol. 92, p. 117403, 03/18/ 2004.

[6] R. E. Collins, *Foundations For Microwave Engineering,* 2nd ed. New York: IEEE Press.

[7] M. J. Gibbons and G. N. Milford, *"Augmented Harmonic Balance stability analysis of nonlinear composite right-left handed transmission lines,"* in Microwave Symposium Digest (MTT), 2011 IEEE MTT-S International, 2011, pp. 1-4.

[8] A. B. Kozyrev and D. W. Van Der Weide, *"Nonlinear wave propagation phenomena in left-handed transmission-line media,"* Microwave Theory and Techniques, IEEE Transactions on, vol. 53, pp. 238-245, 2005.

[9] A. B. Kozyrev and D. W. Van Der Weide, *" Nonlinear left-handed transmission line metamaterials,"* Journal of Physics D: Applied Physics, vol. 41, no. 17, 2008.

[10] D. A. Powell, I. V. Shadrivov, and Y. S. Kivshar, *"Multistability in nonlinear left-handed transmission lines,"* Applied Physics Letters, vol. 92, p. 264104, 2008.

[11] G. N. Milford, *"State-space analysis of left-handed transmission lines,"* in Microwave Symposium (AMS), 2014 1st Australian, 2014, pp. 9-10.